JOURNAL OF PROPULSION AND POWER
Vol. 17, No. 1, January–February 2001

Effect of Sides-Spillage from Airframe on Scramjet Engine Performance

Kouichiro Tani,* Takeshi Kanda,† and Kenji Kudo*
National Aerospace Laboratory, Miyagi 981-1525, Japan
and
Daisuke Akihisa‡
Tohoku University, Miyagi 980-8579, Japan

Precompression by the windward surface of the aerospace plane is necessary for the scramjet operation. However, this precompression causes spillage from the high-pressure windward surface toward the sides of the aerospace plane. To examine the effects of the sides-spillage, performance of a scramjet engine was evaluated with a one-dimensional flow model, and payload to the low Earth orbit was estimated with the flight simulation of an aerospace plane. Prior to the simulation, tests with scramjet inlet models were conducted in a Mach 4 wind tunnel to grasp the primary features of the sides-spillage to support the simulation. The models were inclined from the flow direction to simulate the skewed flow near the side of the plane during sides-spillage. The experiments proved that the aerodynamic performance of the inlet was not affected by the inclination for the given entrance Mach number to the models. However, the mass capture ratio decreased as a result of the reduction of the density of airflow through the expansion. In the numerical estimation the sides-spillage was modeled not to reduce the performance of the inlet, but to reduce mass flow to the inlet. The resulting decrease of delivered airflow to the engine as a result of the spillage reduced the thrust by 15%, while the corresponding payload decreased about 60%. Side fences were effective in preventing spillage.

Nomenclature

A	=	cross section
D	=	drag of the aerospace plane
F	=	net propulsive force of the engine
F_{total}	=	net thrust with drag on the windward surface of the airframe
g	=	acceleration of gravity
h_r	=	height of ramp of the inlet model
I_{sp}	=	specific impulse
L	=	lift of the aerospace plane
M	=	Mach number
m	=	mass of the aerospace plane
$\dot{m}$	=	mass flow rate
P	=	static pressure
P_t	=	total pressure
P_w	=	wall pressure
q	=	dynamic pressure
R	=	radius of the Earth
t	=	time
u	=	velocity
x	=	distance on the Earth surface
y	=	coordinate normal to the top wall in the inlet model
z	=	lateral coordinate in the inlet model, height of aerospace plane
α	=	ramp angle of the inlet model
γ	=	angle of inclination
δ	=	inclination angle of the inlet
θ	=	angle between the engine thrust and the airframe velocity
ρ	=	density

Subscripts

a	=	air
ex	=	inlet exit
i	=	inlet entrance
th	=	inlet throat, i.e., end position of the convergent section of the inlet
∞	=	flight condition
0	=	estimated condition upstream of supposed expansion in front of inlets in inclination
1	=	inlet model entrance
2	=	inlet model exit

Introduction

MANY configurations for the aerospace plane and engine have been proposed.[1–4] The common features of the various aerospace planes in terms of the engine mounting are as follows: 1) multiple engine modules mounted on the airframe, 2) side-by-side arrangement on the windward surface, and 3) precompression of the air by the windward airframe. Because the airframe width is finite, the precompression creates a gradient in pressure between the center and the sides of the airframe. The air spills out from the windward surface to the sides of the airframe. This is designated as *sides-spillage* in the present study. The propagation of the expansion waves from the sides of the airframe affects the amount of airflow delivered to the engine. Figure 1 shows a schematic image of the sides-spillage. The engine modules close to the sides of the airframe are in the expansion waves, and the amount of airflow into the inlet decreases. Also, the inclination of the airflow can affect the engine and the inlet performances.

Inlets for scramjet engines have been studied at many laboratories, institutes, universities, and the National Aerospace Laboratory of Japan.[5–7] The investigations were solely designed to clarify the characteristics of the inlet. However, no study was designed to clarify the effect of the inclined airflow on the inlet performance during the sides-spillage.

In the present study the effects of the sides-spillage were investigated with mission simulations of the operation of the scramjet engine and the flight of the aerospace plane to the low Earth orbit.

Received 1 June 1999; revision received 5 March 2000; accepted for publication 13 April 2000.

*Senior Researcher, Ramjet Propulsion Research Division, Kakuda Research Center, Kakuda.

†Head, Ramjet Systems Section, Ramjet Propulsion Research Division, Kakuda Research Center, Kakuda. Senior Member AIAA.

‡Graduate Student, Department of Aeronautics and Space Engineering, Sendai.

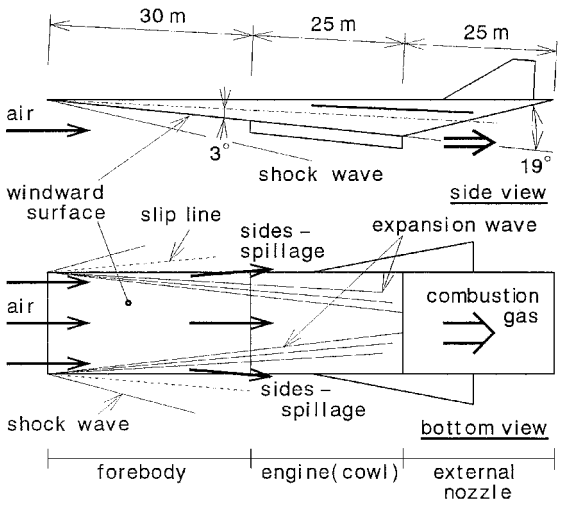

Fig. 1 Schematic diagram of the aerospace plane and the sides-spillage on the aerospace plane.

Prior to the simulation, the effect of the inclination of the airflow as a result of the sides-spillage was investigated with preliminary experiments, and the primary effects on the inlet performance were adopted in the numerical simulations. Several options to prevent the sides-spillage were also discussed.

Numerical Simulation Methods

The impact of the sides-spillage on the engine performance and the payload was evaluated with simulations. A schematic diagram of the airframe for the prediction of the scramjet engine performance is shown in Fig. 1. The airframe had a wedge-shape, two-dimensional nose, and a body width of 15 m. The scramjet engine was on the windward ramp surface of the airframe. The engine was designed at the condition of the flight Mach number of 12. This design condition followed the previous investigation,[8] which showed that the operation of the scramjet engine up to Mach 12 resulted in the maximum payload. The angle of attack was 3 deg, and the windward surface angle from the airframe center axis was also 3 deg. In the simulation of the sides-spillage, both pressure and flow direction in the expanded flow coincided with those after the shock wave at the side of the airframe (Fig. 1). This condition was calculated with the two-dimensional shock-wave relations and the Prandtl–Meyer function.

The height of the scramjet engine was 2 m at the entrance. With this configuration the inlet was in the shock-on-lip condition at Mach 12. A width of the scramjet of 15 m was the same as that of the airframe. The overall contraction ratio of the engine was five. Hydrogen fuel was injected normally into the combustor. In the combustion tests with subscale scramjet engine models, sufficient combustion conditions were attained with normal fuel injection.[9,10] Thus, normal injection was adopted in the simulation. Performance of the scramjet was calculated with the one-dimensional flow model and the two-dimensional flow model. In the calculation the air and the combustion gas were ideal gases with constant specific heats. This model is similar to that used in Ref. 8. Procedure of the calculation was as follows:

1) In the no-spillage case the airflow condition downstream of the shock wave from the leading edge of the airframe was calculated with the two-dimensional shock-wave relations. In the sides-spillage case the airflow was also affected by the expansion waves from the corners of the leading edge of the airframe (Fig. 1). The mean flow condition to the engine was calculated for each case. The boundary layer on the airframe was ignored in the calculation of the flow condition. The ratio of the specific heats and the molecular weight of air were 1.40 and 28.8, respectively.

2) There was no spillage from the inlet itself. The flow condition at the exit of the inlet was estimated one-dimensionally with the mass-conservation relation, the energy-conservation relation, and the inlet kinetic energy efficiency. The effect of the inclined airflow during the sides-spillage was included in the kinetic energy efficiency of the inlet.

3) Quick, stoichiometric combustion occurred in the constant-cross-section duct one-dimensionally above the flight Mach number of 8. Below Mach 8 the equivalence ratio was adjusted so that the Mach number in the combustor was just above unity to avoid thermal choking. The energy increase at combustion for hydrogen mass flow was 121×10^3 kJ · kg^{-1}. The ratio of the specific heats and the molecular weight of the combustion gas were 1.25 and 24.7, respectively.

4) In the internal nozzle the combustion gas expanded isentropically and one-dimensionally. The cross section at the exit of the internal nozzle was the same as that at the entrance of the inlet. The inviscid thrust of the scramjet was calculated with the impulse function at the inlet entrance and at the internal nozzle exit.

5) At the entrance of the external nozzle, the combustion gas expanded to the nozzle wall surface of 19 deg isentropically and two-dimensionally (Fig. 1). The inviscid thrust of the external nozzle was the product of the pressure on the wall surface and the projected wall area. The external nozzle was included in the engine here.

6) A turbulent boundary layer was assumed, and the friction coefficient was set at 0.0025 (Ref. 11). The friction drag was estimated with the inviscid flow conditions estimated at (1–5), and the engine thrust was evaluated by subtracting the friction drag from the sum of the inviscid thrust estimated at 4) and 5).

In the present study the total thrust was defined as the sum of the engine thrust and the drag on the windward airframe surface. Here, the windward airframe surface consists of the surface from the airframe nose to the engine entrance and the outside surface of the cowl. The drag on the airframe was also affected by the expansion waves of the sides-spillage. In the simulation the affected area by the sides-spillage was the windward airframe surface (Fig. 1). The affected area spread, e.g., 8.7 deg from each corner of the airframe leading edge at the flight Mach number of 8 and 6.3 deg at the Mach number of 12, respectively.

In the flight simulation the sides-spillage effect was included during the period of scramjet operation. The simulation methods for the flight of the aerospace plane and the airframe data were the same as those used in the previous investigation.[8] The aerospace plane was treated as a material point. The motion of the plane was within the horizontal and vertical plane. The schematic diagram of the forces is shown in Fig. 2, and the equations used in this study are given as follows:

$$\frac{dx}{dt} = \frac{R}{R+z} \cdot u \cdot \cos\gamma \tag{1}$$

$$\frac{dz}{dt} = u \cdot \sin\gamma \tag{2}$$

$$\frac{du}{dt} = \frac{F \cdot \cos\theta - D}{m} - g \cdot \sin\gamma \tag{3}$$

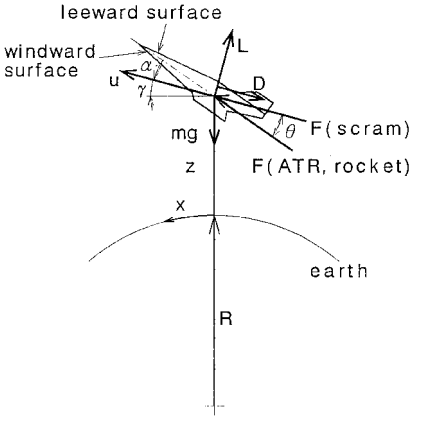

Fig. 2 Force, velocity, and coordinates on aerospace plane.

Table 1 Estimated upstream airflow conditions

Inclined angle, deg	Mach no.	Boundary-layer thickness, mm	Mass flow rate to 30 × 30 mm, kg · s^{-1}	Impulse function to 30 × 30 mm, N	Density kg · m^{-3}
0	3.95	8.7	0.38	260	0.69
3	3.73	7.0	0.47	320	0.85
4.5	3.63	6.3	0.52	360	0.94

$$\frac{d\gamma}{dt} = \frac{F \cdot \sin\theta + L}{m \cdot u} - \frac{g \cdot \cos\gamma}{u} + \frac{u \cdot \cos\gamma}{R + z} \tag{4}$$

$$\frac{dm}{dt} = -\frac{F}{I_{sp}} \tag{5}$$

From the takeoff to the flight Mach number of 6, a hydrogen-fueled air-turbo-ramjet (ATR) propulsion system[12] was used. From Mach 6 to around Mach 12, the scramjet was applied. After the operation of the scramjet engine, the LOX/LH_2 rocket engine[13] was used to achieve the low Earth orbit at 100-km altitude. The flight dynamic pressure was equal to 100 kPa during the operation of ATR or the scramjet, except at the takeoff.

The initial mass of the aerospace plane was 460 tons at the horizontal takeoff. The weight of each part of the aerospace plane, e.g., airframe, engines, was estimated by a weight-analysis program,[14] and modification was applied to its results.[8] For example, 51 tons were adopted for the mass of the airframe, whereas the masses of the scramjet, ATR, and the rocket engine were 2, 6, and 0.7% of the initial mass of the aerospace plane, respectively.

Experimental Apparatus

To investigate the effects of the inclination of the airflow as a result of the sides-spillage on inlet performance, the preliminary test with three inlet models was conducted in a Mach 4 wind tunnel.[1] The inflow total pressure and the total temperature were 2.0 MPa and 290 K, respectively. The cross section on dimensions of the test section was 10 by 10 cm. The Reynolds number was 9×10^7 m^{-1}. The thickness of the boundary layer at 99% of the freestream velocity was 8.7 mm at the entrance of the inlet model.

Figure 3 shows the inlet model, which employed both side-wall compression and ramp compression. The end of the ramp surface coincided with the end of the convergent section of the side wall. Three ramp configurations were prepared, corresponding to $\alpha = 0$, 5.7, and 8.3 deg. The heights of the ramps h_r were 0, 10, and 15 mm, respectively. The overall contraction ratios of the models were 2, 3, and 4, respectively. Side-wall sweep-back angles were 45 deg. The shape of the model was designed for possible variable geometry such that the top wall could move toward the cowl in the convergent section. The three ramps corresponded to the possible positions of the top wall. In the present tests the cowl leading edge was located at the end of the convergent section of the inlet. Downstream of the convergent duct in the inlet was a constant cross-sectional duct, which simulated an isolator.

The entire inlet model was installed on a rotating plate. The plate provided inclination angles of 0, 3, and 4.5 deg to the freestream. The inclination direction was as shown in Fig. 3. In the inclined condition, the right side wall was on the windward side, and the angle to the airflow of the right side wall increased. At the inclination of 4.5 deg, the leeward surface of the left side wall had a negative angle to the freestream.

During the sides-spillage, the spilled flow inclines parallel to the slip line (Fig. 1). According to the estimation, the angle of the slip line was about 3 deg in the scramjet operation from the flight Mach number 6 to 12. Therefore, the effect of the inclined flow during the sides-spillage was simulated with the inclination angles of the present tests.

Wall pressure in the model and pitot pressure at the exit of the model were measured by a mechanical pressure scanner with 0.5 s per pressure port. Pitot pressure was measured at 45 points in the no-ramp model. The pressures were normalized by the total pressure

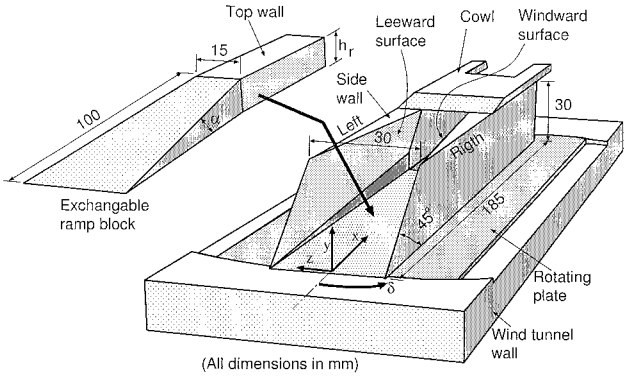

Fig. 3 Inlet models used in the experiments.

of the wind-tunnel reservoir. The accuracy of the wall pressure and the pitot pressure were ±0.001 and ±0.002 in the normalized form, respectively. The pitot pressure and the side-wall static pressure at the same height as the pitot tube were used to estimate the total pressure.

The test conditions with the inclination of the model correspond to those of the engine module close to the sides of the airframe, which experiences inclined and expanded airflow. In the evaluation of the inlet performances, the airflow condition upstream of the inclination, i.e., the condition upstream of the supposed expansion waves, should be adopted as a reference condition. The condition was estimated based on the following assumptions:

1) The inclined angle of the airflow through the supposed expansion waves was identical to the angle of the rotating plate.

2) The velocity profile in the boundary layer followed the power law, and the profile did not change throughout the expansion.

3) The mass flow rate in the boundary layer was conserved throughout the expansion.

The upstream Mach number and velocity at the edge of the boundary layer were estimated based on the Prandtl–Meyer function and assumption 1). The upstream boundary-layer thickness was calculated based on assumptions 2) and 3). The airflow condition upstream of the expansion could be reasonably estimated with the preceding procedure. In the procedure the momentum conservation in the boundary layer was ignored. This resulted in an error in the momentum balance of 0.7% when the air was inclined at 4.5 deg. Table 1 shows the estimated upstream airflow conditions at each inclination.

Experimental Results and Discussion

Wall Pressure and Total-Pressure Distributions

The pressure distributions at the exit of the isolator in the no-ramp model are shown in Fig. 4. In the figure the top wall is located at $y = 0$ mm and the cowl at $y = 30$ mm. Near the top wall and near the cowl, there was a shift in pressure level because of the inclination. Near the top wall the impinging point of the cowl shock wave on the top wall moved upstream with the inclination. Because the cowl shock wave was skewed as a result of the nonuniformity of the incoming flow, the pressure level on the left side was elevated. The level on the right side showed less change. The pressure distribution was skewed with the inclination.

Figure 5 shows the total-pressure distributions at the exit plane of the no-ramp model. The right and left side walls were at $z = 7.5$

Table 2 Inlet model performances

Ramp angle of inlet model, deg	Inclination, deg	Average exit Mach no.	Total-pressure efficiency	Mass capture with sides-spillage	Mass capture of inlet	Impulse function with sides-spillage	Impulse function of inlet
0	0	2.74	0.53	0.74	0.74	0.627	0.627
	3	2.75	0.55	0.59	0.74	0.506	0.624
	4.5	2.81	0.58	0.54	0.75	0.469	0.640
5.7	0	2.27	0.37	0.37	0.37	0.278	0.278
	3	2.36	0.34	0.30	0.38	0.267	0.295
	4.5	2.47	0.40	0.29	0.41	0.239	0.327
8.6	0	2.36	0.32	0.29	0.29	0.233	0.233
	3	2.31	0.30	0.23	0.29	0.186	0.229
	4.5	2.37	0.33	0.22	0.31	0.181	0.247

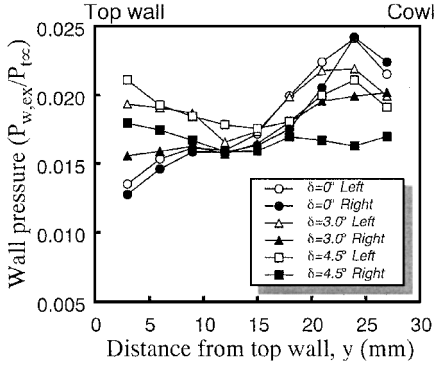

Fig. 4 Pressure distributions on the side wall at the exit of the no-ramp model.

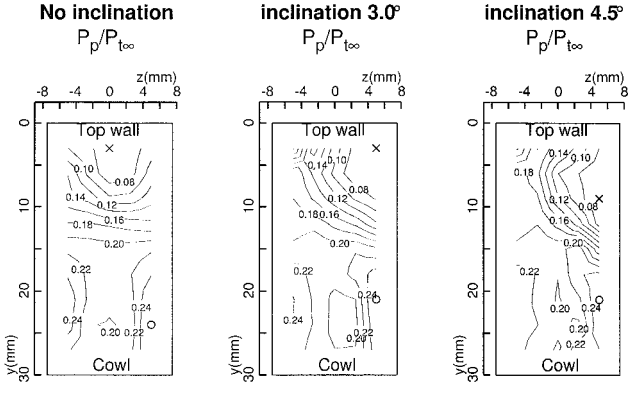

Fig. 5 Total-pressure distributions at the exit of the no-ramp model.

and −7.5 mm, respectively. In the figure the cross and the circle represent the positions of the lowest and the highest total pressures, respectively. When there was no inclination, the distribution was approximately symmetrical. Near the top wall there was a low total-pressure region, which was caused by the thick boundary layer. The total pressure was high around the center, then decreased near the cowl. With the inclination the area with high total-pressure spread on the right side between the mid and the cowl, and the contour lines were skewed.

Inlet Performance

Table 2 lists average Mach numbers, total-pressure efficiencies, mass capture ratios, and impulse functions at the exit of the models. In the table mass capture ratio with sides-spillage and impulse function ratio with sides-spillage used the flow conditions upstream of the supposed expansion listed in Table 1 as references. The estimation method of the flow condition upstream of the expansion was described in the section Experimental Apparatus.

(mass capture ratio with sides-spillage)

$$= \frac{\text{(mass flow rate at the inlet exit)}}{\text{(mass flow rate upstream of the supposed expansion)}}$$

$$= \frac{\int \rho_2 u_2 \, dA_2}{\int \rho_0 u_0 \, dA_1}$$

(impulse function ratio with sides-spillage)

$$= \frac{\text{(impulse function at the inlet exit)}}{\text{(impulse function upstream of the supposed expansion)}}$$

$$= \frac{\int \left(\rho_2 u_2^2 + P_2\right) dA_2}{\int \left(\rho_0 u_0^2 + P_0\right) dA_1}$$

Mass capture ratio of inlet and impulse function ratio of inlet used flow conditions at the entrance of the inlet model as the references. In other words, mass capture ratio of inlet and impulse function ratio of inlet represented the sole performance parameters in the inlet in the inclined flow.

(mass capture ratio of inlet)

$$= \frac{\text{(mass flow rate at the inlet exit)}}{\text{(mass flow rate at the inlet entrance)}}$$

$$= \frac{\int \rho_2 u_2 \, dA_2}{\int \rho_1 u_1 \, dA_1}$$

(impulse function ratio of inlet)

$$= \frac{\text{(impulse function at the inlet exit)}}{\text{(impulse function at the inlet entrance)}}$$

$$= \frac{\int \left(\rho_2 u_2^2 + P_2\right) dA_2}{\int \left(\rho_1 u_1^2 + P_1\right) dA_1}$$

With inclination to the airflow, the total-pressure efficiency and the Mach number increased. However, the changes caused by the inclination were small. The measured total-pressure efficiency corresponded to a kinetic energy efficiency of 0.95 in the no-ramp model. Mass capture ratio of inlet did not change significantly by the inclination, i.e., the inclination of the airflow to the inlet did not change the inlet spillage significantly. Impulse function ratio of inlet did not change significantly by the inclination either. This means that the stream thrust function was approximately the same in each ramp model. Although the airflow remained skewed, the average performance of the inlet did not change significantly because of the inclination of the incoming airflow.

Mass capture ratio with sides-spillage decreased with the inclination. Because the density decreased significantly through the supposed expansion waves, the estimated mass flow rate upstream of the expansion waves became larger with inclination as listed in Table 1. Beside the sides-spillage, the mass flow rate at the throat of the inlet is reduced by spillage from the open bottom of the inlet, and this

spillage changes because of the Mach number and the shock-wave structure in the model. In the current experiment, the change of the entrance Mach number as a result of the inclination was, at most, 0.3, as listed in Table 1. According to the calculated results using the two-dimensional shock-wave relations,[15] a shift of the entrance Mach number of 0.3 for Mach 4 would cause the change of the mass capture ratio by up to 5%. The changes in the mass capture ratio with expansion listed in Table 2 were much larger than 5%, indicating that the decrease of the mass capture ratio was primarily caused by the decrease of the density throughout the expansion. Impulse function ratio with sides-spillage also decreased primarily because of the decrease of the mass capture ratio. This means that the spilled impulse function increases as a result of the sides-spillage upstream of the inlet, and thus the engine thrust decreases.

In the model with the ramp top wall, spillage was increased by the shock wave from the ramp. In the ramp model, the cowl should be extended forward to prevent spillage. When the cowl was extended upstream 20 mm in the 5.7-deg ramp model, mass capture ratio of inlet increased to 0.56 in a no-inclination condition. In the model with the ramp, the total-pressure ratio and the impulse function ratios were small. It was caused by the spillage of the primary flow by the ramp shock wave.

Simulation Results and Discussion

The experiments proved that the sides-spillage decreased the mass flow rate into the inlet significantly, but did not affect the aerodynamic performance of the inlet significantly. In the simulation, only the airflow to the engine was reduced by the sides-spillage. The assumption of the constant kinetic energy efficiency of the inlet regardless of the sides-spillage was reasonable in the following simulation. The kinetic energy efficiency of inlets is nearly constant with flight Mach number.[16] The kinetic energy efficiency of the inlet was set to be 0.98, which was attained by the empirical equation.[17] Approximately the same value of the inlet was attained in the tests with the subscale scramjet model.[9,10] The low efficiency in the present experiments of 0.95 was caused by the thick boundary layer.

Engine Performance

Figure 6 shows the thrust coefficients of the engine models. The coefficient is defined as the ratio of the total thrust to the product of the flight dynamic pressure and the projected cross section of the engine at the entrance. The results with side fence and side ramp will be mentioned later. Figure 7 shows the mass flow rate into the engine, which is nondimensionalized by the product of the mass flux of the freestream and the projected cross section of the engine at the entrance.

The thrust coefficient of the engine with the sides-spillage was 15% lower than that of the engine with no spillage. This was caused by the smaller mass flow rate into the engine, as shown in Fig. 7. The small discrepancy between the trends in thrust coefficients and mass flow rates was caused by the difference in pressure on the windward airframe surface. Figure 8 shows the breakdown of thrust/drag at a flight Mach number of 10. The effect of the sides-spillage slightly decreased the pressure drag of the aerospace plane. However, the decline in the engine-produced thrust was much larger than the decrease in drag on the airframe.

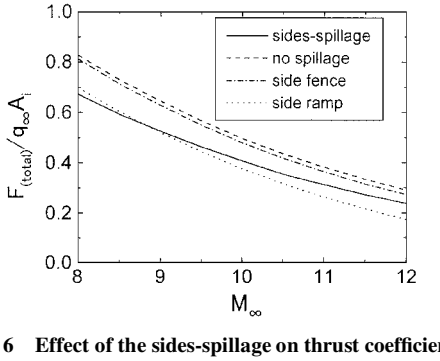

Fig. 6 Effect of the sides-spillage on thrust coefficient.

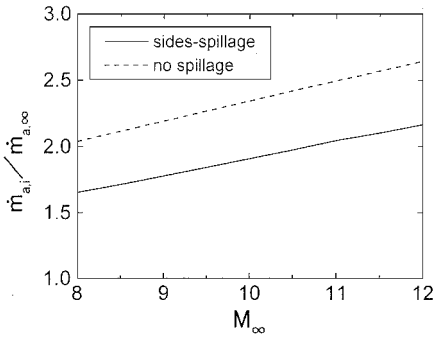

Fig. 7 Effect of the sides-spillage on the mass flow rate into the scramjet engine.

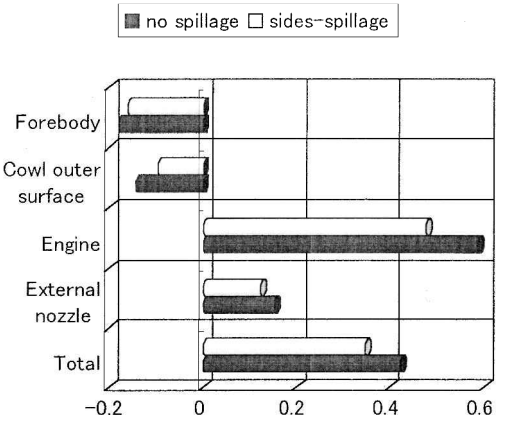

Fig. 8 Thrust/drag contents of the aerospace plane at a flight Mach number of 10.

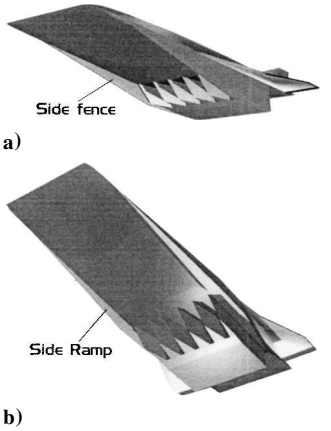

Fig. 9 Schematic diagrams of a) an aerospace plane with side fences and b) a plane with side ramps.

To prevent sides-spillage, side fences and side ramps, as shown in Fig. 9, are options. The total thrust with each option was calculated to clarify its effectiveness. The fences were attached to the sides of the airframe from the nose of the airframe to the entrance of the engine. No propagation of the expansion waves from the sides of the airframe was assumed. The thickness of the fences and the pressure drag on them were neglected. The friction drag on the fences was counted in the total thrust.

The side surfaces of the body for the model with the side ramps had an angle of 6 deg from the flight direction. This angle was chosen to be the same as the sum of the windward airframe angle and the angle of attack. With this configuration, the pressure on the windward surface was expected to be approximately the same as that on the surface of the side ramps, which means that there was no formation of expansion waves to the windward surface from the sides of the airframe and no spillage. The effects of the pressure

Table 3 Contents of mass ratio in aerospace plane

Property	Fuel	Oxidizer	Fuel tank	Oxidizer tank	Airframe	Engines	Payload
No spillage	0.295	0.451	0.033	0.008	0.111	0.087	0.015
With sides-spillage	0.308	0.443	0.035	0.007	0.111	0.087	0.008

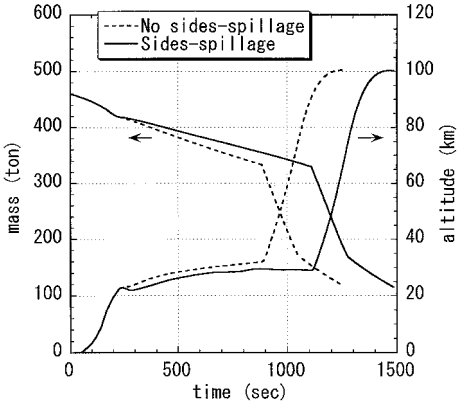

Fig. 10 Flight conditions of the sides-spillage case and no-spillage case.

on the leeward side of the airframe and of the formation of the secondary flow on the pressure on the side ramps were neglected. The pressure drag on the ramp surfaces was included in the total thrust.

The resulting engine performances are also shown in Fig. 6. The friction drag on the fences decreased the thrust slightly from that of the model with no sides-spillage, and the result showed the fences to be effective for suppression of the decrease in thrust caused by the sides-spillage. When the fences are attached to the airframe, additional secondary flows may appear, e.g., vortex flow at the corner of the airframe and the fences. This can cause engine-starting problems. By making the gap between the inlet and the side fence, the vortex flow at the corner will be evacuated outside the engine. The side ramps increased pressure drag, and the thrust was lower than that with the sides-spillage. The attachment of the side ramps was a negative factor for thrust.

Payload Estimation

An additional drag or weight penalty as a result of employment of modification devices, e.g., side fences or side ramps, was not included in the flight simulation. In the present study, the scramjet operated up to a flight Mach number of 11 in both the sides-spillage and the no-spillage conditions. When the scramjet was used up to Mach 11, the payload became maximum in both conditions. Figure 10 shows the flight conditions of the sides-spillage case and the no-spillage case. Table 3 lists the contents of the mass ratios of the aerospace plane.

The effect of the sides-spillage was included during the scramjet operation in this study. The operating time was longer with the sides-spillage case because of the low thrust. In addition, the fuel consumed during the scramjet operation was increased by 6.5 tons with the sides-spillage. Finally, the payload for the scramjet vehicle with the sides-spillage was 3.9 tons, whereas that with no-spillage was 6.9 tons. Hence, the payload was 43% lower than that with no-spillage. Assuming the aerospace plane went into an orbit of 200 km, the payloads of both operations were 2.0 tons with the sides-spillage and 4.9 tons with no-spillage. The payload level became smaller at the higher orbit, and the ratio of the payloads further decreased because of the sides-spillage. Each part of the aerospace plane can become heavier than the predicted value. Then the payload of each mission will become smaller, and the ratio of the payloads further decreased because of the sides-spillage.

If lightweight side fences under 3 tons could be manufactured, prevention of sides-spillage would be beneficial. The volume of a side fence was about 0.3 m^3, assuming a thickness of 1 cm. If the nickel-alloy panel-structure with 1-mm average thickness and ceramic tile are used for the fences, the weights of the structure and the tile become 530 and 100 kg, respectively. The weight of the fences becomes 630 kg, and the actual weight will be around the present estimation. Attachment of the fences is advantageous.

Concluding Remarks

The authors investigated the effects of the sides-spillage, i.e., the spillage of the airflow by propagation of expansion waves from the sides of the airframe, on the performance of the scramjet and the aerospace plane. The effect on the inlet performances by the sides-spillage was preliminarily investigated in a Mach 4 wind tunnel, and the primary features of the sides-spillage were attained. Then numerical simulations of the scramjet engine and the flight of the aerospace plane were conducted. The investigations clarified the following points:

1) The inclination of the incoming airflow by the sides-spillage had only a small effect on the average performance of the inlet models.

2) The major effect of the sides-spillage was the decrease of the mass capture ratio.

3) The thrust decreased by 15% as a result of the sides-spillage caused by the decrease of the airflow rate, and the payload also decreased to 60% due to the sides-spillage.

4) Side fences were beneficial to prevent the sides-spillage. The attachment of the side ramps was a negative factor for thrust.

Acknowledgments

The authors wish to thank Yoshinori Futonagane, graduate student of Tohoku University and currently Researcher of Toyota Motor Company, Ltd., for help in the experiments.

References

[1] Huebner, L. D., "Computational Inlet-Fairing Effects and Plume Characterization on a Hypersonic Powered Model," *Journal of Aircraft*, Vol. 32, No. 6, 1995, pp. 1240–1245.

[2] Hozumi, K., Watanabe, S., and Nomura, S., "Aerodynamic Studies on Space Plane Configuration at Hypersonic Speed," *Proceedings of the 17th International Symposium on Space Technology and Space Science (ISTS)*, Committee of ISTS, Tokyo, 1990, pp. 1365–1376.

[3] Weinreich, H.-L., Grallert, H., Parkinson, R., and Berry, W., "Studies of a Scramjet-Propelled, Horizontal Launch and Landing, Single-Stage-to-Orbit Launcher," AIAA Paper 93-5053, Nov. 1993.

[4] Lockwood, M. K., Hunt, J. L., Kabis, H., Moses, P., Pao, J.-L., Yarrington, P., and Collier, C., "Design and Analysis of a Two-Stage-to-Orbit Airbreathing Hypersonic Vehicle Concept," AIAA Paper 96-2890, July 1996.

[5] Kanda, T., Komuro, T., Masuya, G., Kudo, K., Murakami, A., Tani, K., Wakamatsu, Y., and Chinzei, N., "Mach 4 Testing of Scramjet Inlet Models," *Journal of Propulsion and Power*, Vol. 7, No. 2, 1991, pp. 275–280.

[6] Tani, K., Kanda, T., Kudou, K., Murakami, A., Komuro, T., and Ito. K., "Aerodynamic Performance of Scramjet Inlet Models with a Single Strut," AIAA Paper 93-0741, Jan. 1993.

[7] Tani, K., Kanda, T., and Tokunaga, T., "Starting Characteristics of Scramjet Inlets," *Proceedings of the 11th International Symposium on Air Breathing Engines*, AIAA, Washington, DC, 1993, pp. 1071–1080.

[8] Kanda, T., and Kudo, K., "Payload to Low Earth Orbit by Aerospace Plane with Scramjet Engine," *Journal of Propulsion and Power*, Vol. 13, No. 1, 1997, pp. 164–166.

[9] Kanda, T., Hiraiwa, T., Mitani, T., Tomioka, S., and Chinzei, N., "Mach 6 Testing of a Scramjet Engine Model," *Journal of Propulsion and Power*, Vol. 13, No. 4, 1997, pp. 543–551.

[10] Kanda, T., Sunami, T., Tomioka, S., Tani, K., and Mitani, T., "Mach 8 Testing of a Scramjet Engine Model," *Journal of Propulsion and Power*, Vol. 17, No. 1, 2001.

[11]Swithenbank, J., "Hypersonic Airbeathing Propulsion," *Progress in Aeronautical Sciences*, 1st ed., Vol. 8, Pergamon, Oxford, England, U. K., 1967, p. 245.

[12]Sakata, K., Yanagi, R., Shindo, S., Minoda, M., and Nouse, H., "Conceptual Study on Air-Breathing Propulsion for Space Plane," *Proceedings of the 16th International Symposium on Space Technology and Science*, Committee of International Symposium on Space Technology and Science, Tokyo, 1988, pp. 107–112.

[13]Kanmuri, A., Kanda, T., Wakamatsu, Y., Torii, Y., Kagawa, E., and Hasegawa, K., "Transient Analysis of LOX/LH2 Rocket Engine (LE-7)," AIAA Paper 89-2736, July 1989.

[14]Glatt, C. R., "WAATS—A Computer Program for Weight Analysis of Advanced Transportation Systems," NASA CR-2420, Sept. 1974.

[15]Trexler, C. A., and Souders, S. W., "Design and Performance at a Local Mach Number of 6 of an Inlet for an Integrated Scramjet Concept," NASA TN D-7944, Aug. 1975.

[16]Kerrebrock, J. L., "Some Readily Quantifiable Aspects of Scramjet Engine Performance," *Journal of Propulsion and Power*, Vol. 8, No. 5, 1992, pp. 1116–1122.

[17]Heiser, W. H., Pratt, D. T., Daley, D. H., and Mehta, U. B., "Hypersonic Airbreathing Propulsion," edited by J. S. Przemieniecki, AIAA Education Series, AIAA, Washington, DC, 1994, p. 225.